Controlled double-slit electron diffraction

Roger Bach[1], Damian Pope[2], Sy-Hwang Liou[1] and Herman Batelaan[1]

[1]Department of Physics and Astronomy, University of Nebraska-Lincoln, Theodore P. Jorgensen Hall, Lincoln, NE 68588, USA.
[2]Perimeter Institute for Theoretical Physics, 31 Caroline ST N, Waterloo, Ontario, Canada N2L2Y5.

E-mail: hbatelaan2@unl.edu

Supplementary Information

Table of Contents:

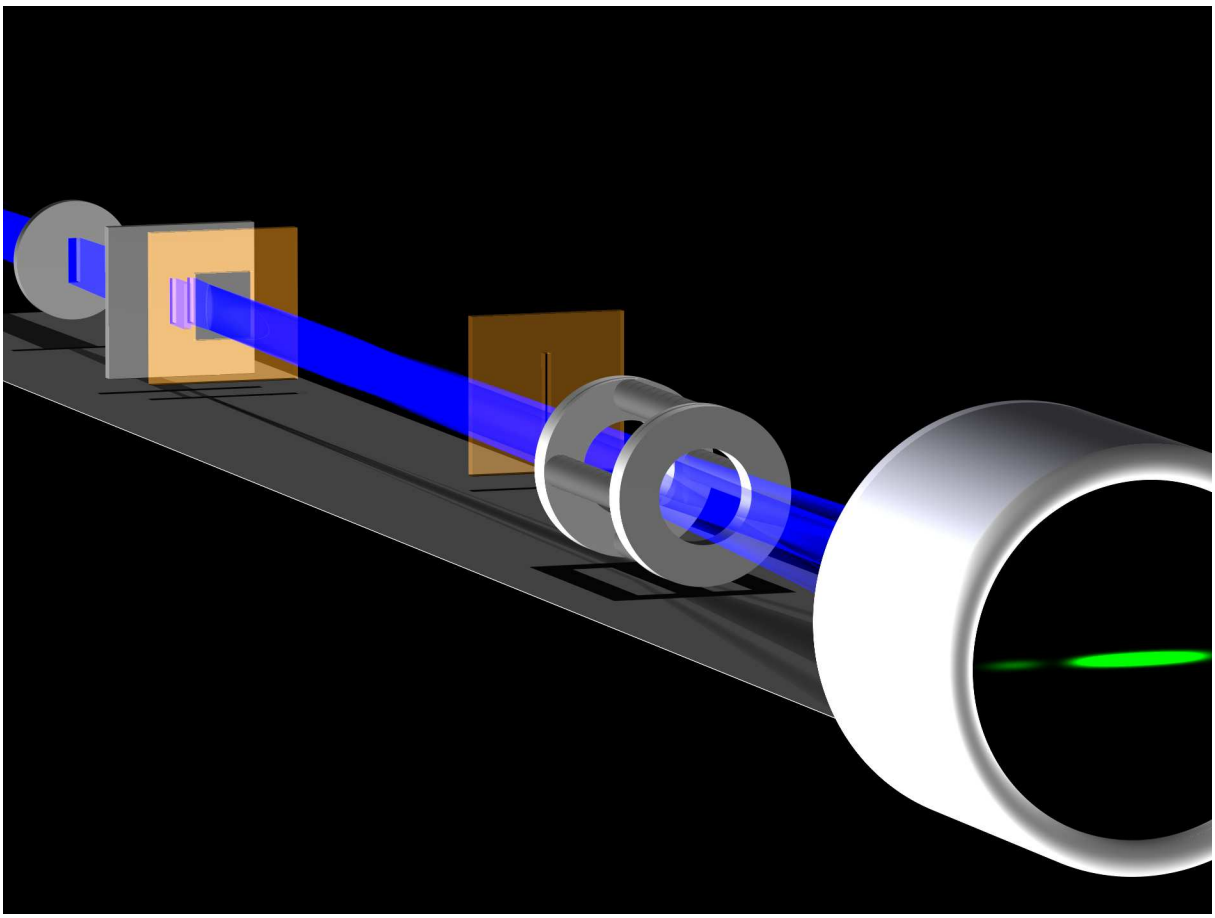

Figure S1. Illustration of the experimental setup. The electrons are first collimated by a 2 ± 0.5 μm collimation slit. Then the electrons pass through the double slit, consisting of two 62.3 ± 4.0 wide slits separated center-to-center by 272.6 ± 17.6 nm. A movable mask, 4520 nm wide, is used to block none, one, or both of the slits. The resulting pattern can either be sampled by a movable detection slit, or magnified by a electrostatic quadropole lens and imaged on a two-dimensional microchannel plate and phosphorus screen

1 Full description of setup

The experiment was performed in a stainless steel vacuum chamber at a pressure below 10^{-7} Torr. The system has two layers of magnetic shielding. The magnetic fields inside the shielding were on the order of 5 mG. A schematic of the experimental system is illustrated in figure S1. An electron gun constiting of a thermionic tungsten filament source and several electrostatic lenses was used to emit and aim an electron beam. The electron beam was collimated by a 2 ± 0.5 μm wide $\times$ 100 μm tall slit located 15 cm from the end of the electron gun. The double slit was located 30.5 cm for the collimation slit. A mask that could be moved on a nanometer scale, was placed 240 μm away from the double slit. A movable detection slit, 5 μm wide $\times$ 3 mm tall, was located 240 ± 5 mm from the double slit. Located after the detection slit was a variable electrostatic quadropole lens. The electrons were detected with a 18 mm diameter two-dimensional microchannel plate

(MCP) and phosphorus screen (Beam Imaging Solutions' BOS-18-OPT01). An external low light camera (Watec's WAT-902B) was used to record the image from the phosphorus screen.

The mask was used to block none, one, or both slits of the double slit. The mask and double slit were mounted together to limit the relative motion of the two. The mask was held securely in a frame the could slide back and forth and was controlled by a piezoelectric actuator (Thorlabs' AE0505D16F). The voltage used to drive the actuator was used to infer the position.

The detection slit allowed for the sampling of the diffraction pattern in the horizontal direction, as well as being able to be moved out of the way to allow the pattern to be imaged directly on the MCP detector. Sampling was accomplished by moving the diffraction pattern across the 5 μm slit by a set of electrostatic deflection plates (not shown in figure S1). The deflection plates were separated by 2 cm and were composed of $\sim$5 cm square plates with the center located 14 cm from the double slit, and 10 cm before the detection slit. The voltage on the deflection plates was calibrated by moving the detection slit a known amount and repeating a pattern. Moving the detection slit or deflecting the pattern give essentially identical patterns but using the deflection plates allow for smaller horizontal steps to be taken. This detection scheme was similar to Barwick et al. [S1].

The electrostatic quadropole lens was used to magnify the electron patterns. The lens consisted of two grounded circular end plates with four voltage addressable rods in between, arranged as shown in figure S1. Each opposite pair was held at the same potential, with the horizontal pair being at +V and the vertical pair being at -V. This allows expansion of the pattern in horizontal direction but depending on voltage either contraction or expansion in the vertical direction. The lens was necessary because the entire size of the non-magnified patterns would be comparable to resolution of the two-dimensional detector MCP detector.

2 Measurements and fits

The double-slit and mask were made by focused ion beam (FIB) milling 100-nm-thin silicon-nitride membrane windows. The FIB milling was performed on a 30-keV Ga^+ system (FEI's Strata 200xp). Scanning electron microscope (SEM) images were taken on an electron beam lithography system (Zeiss Supra 40). The images are shown in figure 1 inset 1 and 2. The dimensions obtained using the SEM images are shown in table S1.

The detection slit (see figure S1) allowed for the acquisition of diffraction patterns with resolution of $\sim$5 μm (see figure S2a). This data was fit with a least-squares procedure using [S2]

$$I = A_0 + A\left(\frac{\sin(\alpha x)}{\alpha x}\right)^2 (1 + V\cos(2 * \beta x)), \tag{S1}$$

where $\alpha = \frac{\pi a}{\lambda D}$ and $\beta = \frac{\pi d}{\lambda D}$. The de Broglie wavelength (λ) was 50.07 $\pm$ 0.13 pm and the propagation distance (D) was 240 $\pm$ 5 mm. A_0, A, a, d, and V are fit parameters with a representing the slit width, d the center-to-center separation, and V the visibility

	a (nm)	d (nm)	$\frac{d}{a}$	Mask (nm)
SEM	64.6	282.7	4.38	4680
Detection Slit	69.9 ± 3.3	272.6 ± 11.3	$3.90 \pm .09$	_____
MCP Detector	62.3 ± 4.0	272.6 ± 17.6	$4.38 \pm .01$	_____
Simulation	62.3	272.6	4.38	4520

Table S1. Double slit specifications. The dimensions found using different measurement techniques and the dimensions used in the quantum mechanical simulation. The width of each of the slits in the double-slit is a and d is the separation of the slits. The majority of the errors in the width and separation come from the uncertainty in the wavelength, propagation distance, and fitting. The error in the ratio is from the uncertainty in the fitting

parameter, $V = \frac{(I_{max}-I_{min})}{(I_{max}+I_{min})}$, of the diffraction pattern. A normalized fit of the pattern is shown in figure S2a. The width and separation dimensions found are listed in table S1. The visibility parameter was $0.819 \pm .032$.

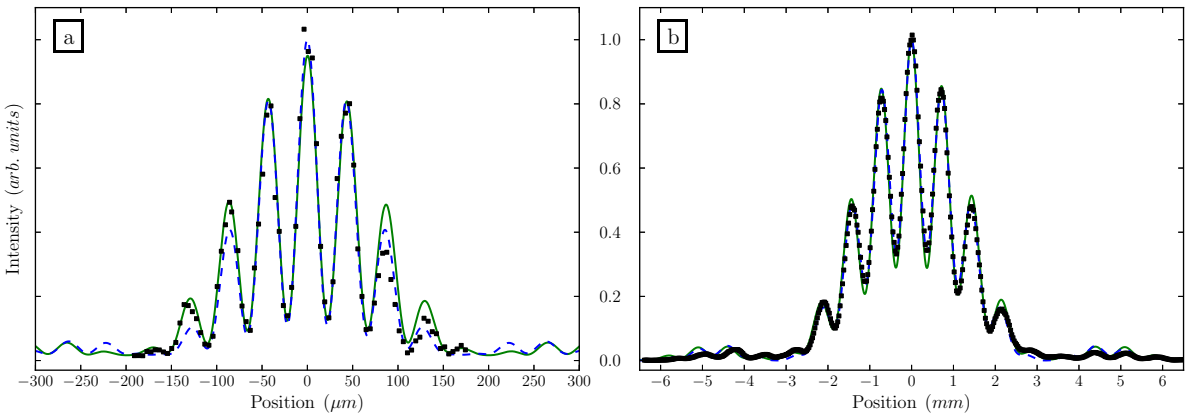

Figure S2. Diffraction recorded at the detection slit (a) and the MCP detector (b). The squares (black) represent the experimental data, the solid line (green) represent the results of the path integral model, and the dashed line (blue) represents the fit of two partially coherent sources.

One drawback of using the detection slit was the low count rate. This caused long acquisition times (∼130 sec/point, >3 hr. total) and limited the spatial range of the diffraction pattern we were able to sample. Drifts in the electron emission current could change the relative count rate as the pattern was acquired (left to right). This could be an explanation why the diffraction pattern in figure S2a shows an asymmetry between the left and right sides. These effects can cause the a parameter to be an overestimate of the actual slit width, but should not affect the d parameter because it is only dependent on the location of the peaks and not the heights.

The same fitting procedure, using equation (S1), could be used on the data acquired from the MCP detector (see figure 3 and figure S2b). Since the quadropole only magnifies the horizontal dimension the vertical dimension was summed up to perform the fit in one dimension. Now the fitting parameters a and d will consist of a magnification factor as well as the slit width and separation. To determine the magnification factor both d parameters (detection slit and MCP detector) were set equal to each other. For the voltages used during the acquisition of data in figure 2 (and figure S2b) the magnification factor was 16.58 $\pm$ 0.90. This allows the slit widths and separation to be determined, they are given in table S1. The visibility parameter was 0.477 $\pm$ .0034.

The main reason for the drop in visibility between the detection slit and MCP detector (figure S2a and b) was the increase in detection resolution. The MCP detector and camera setup had a resolution of 238.2 $\pm$ 6.6 μm. This was determined by fitting the individual electron detection events and determining the appropriate detection resolution.

All three of these methods gave slightly different values for the slit widths and separation. One parameter that could be determined independently in each situation was the ratio of $\frac{d}{a}$ (see table S1). This values is independent from the calibration of the SEM or the magnification factor. The SEM and MCP Detector both obtained the same ratio. There is a 4% difference between the width and separation measurements.

3 Path integral simulation

To compare with experimental results, a quantum mechanical numerical simulation was produced. The theoretical description of the physical system is based on Feynman's path integral formulation [S3]. The simulation was similar in construction as Barwick et al. [S1] and Caprez et al. [S4]. The wave function $\Psi(x)$ was propagated from one plane to the next, i.e., the plane of the collimation slit, double slit, mask, detection plane. This was done by

$$\Psi_f(x) = \int K_{i\to f}(x', x)\Psi_f(x')dx'. \tag{S2}$$

The coordinate system is chosen so that the x-axis is horizontal in figure S1 and is perpendicular to the beam propagation axis, which is the z-axis. The kernel in equation (S2) is given by

$$K_{i\to f}(x', x) = \exp\left(i\frac{S(x', x)}{\hbar}\right), \tag{S3}$$

where S is the classical action. For this setup the wavefunction propagates in free space between the planes. For that propagation, the action simplifies to

$$S(x', x) = 2\pi\frac{\sqrt{(x'-x)^2 + (z'-z)^2}}{\lambda}, \tag{S4}$$

where λ is the de Broglie wavelength.

At the planes, the wavefunction is modified by

$$\Psi_{out}(x) = A(x)\exp(i\phi(x))\Psi_{in}(x), \tag{S5}$$

where A describes the physical interaction of the plane and ϕ describes the electromagnetic interaction with the plane. For example, at the double slit plane

$$A(x) = H\left(x + \frac{d}{2} + \frac{a}{2}\right) \cdot H\left(-x - \frac{d}{2} + \frac{a}{2}\right) + H\left(x - \frac{d}{2} + \frac{a}{2}\right) \cdot H\left(-x + \frac{d}{2} + \frac{a}{2}\right), \quad \text{(S6)}$$

where a and d are the double slit dimensions and H is the Heaviside function. For a full description of the electromagnetic interaction see Barwick et al. [S1]. At the collimation slit and mask an image charge potential was added. At the double slit an additional random potential was added. The values describing the interaction were identical to the ones used by Barwick et al. except the full width half max of the amplitude of the random potential. The values are summarized in table S2. The physical system that motivates the random potential is based on contact potentials. The metal coating that was used on the gratings by Barwick et al. was different that the coating used during the current experiment. This difference warranted small changes in amplitude of the random potential to describe the interaction accurately.

	Image Charge	Random Potential			
		Width		Amplitude	
	q_{eff}	Mean	FWHM	Mean	FWHM
Barwick et al. [S1]	$0.13e$	250 nm	250 nm	0 eV	0.350 eV
Current Simulation	$0.13e$	250 nm	250 nm	0 eV	0.225 eV

Table S2. Comparison of simulation parameters between current simulation and the simulation done by Barwick et al [S1].

To incorporate the electron gun into the simulation incoherent sources were added. A point source on the collimation slit was propagated through the setup and then incoherently added up with other point sources from the collimation slit (See Barwick et al. for full description). This considers the collimation slit to be illuminated fully incoherently. After the incoherent addition the resulting probability distribution represents what the detection slit samples.

The parameters for the double slit used in the simulations are listed in table S1. The diffraction pattern calculated at the detection slit is shown in figure S2a with an offset to account for background.

To simulate the pattern obtained at the MCP detector the quadrople and detector needed to be accounted for. To do this the magnification factor, used in section 2, was multiplied with the value of the x coordinate and then the probability distribution was convoluted with the MCP detector resolution. The probability distribution calculated at the MCP detector is shown in figure S2b. There is excellent agreement between the simulation and the experiment. The small asymmetry between the right and left orders is gone because with this detection method the pattern is built up all at ounce and variation in the initial beam's intensity will not affect each side differently. There is a slight discrepancy on the positions of the leftmost orders. This is most likely due to the

interaction of the quadropole. That section of the pattern was not magnified uniformly as the rest of the pattern was.

To represent the mask movement and fully reproduce the patterns on the MCP detector, the simulation was performed multiple times with the mask in a different position. Then the probability distribution was multiplied by a Gaussian in the y direction. The distribution was made into a false colour plot in the exact same manner as the data was. A transformation function was used to highlight outer orders by over saturating the central orders

$$A_{out}(x, y) = 1 - \exp\left(-20A_{in}(x, y)\right), \tag{S7}$$

where A_{in} and A_{out} are the before and after probability distributions respectively and both have values between 0 and 1. The value of 20 was chosen for visual appearance.

The different positions of the mask are shown in figure S3. For comparison purposes the image is identical in it's layout and positions of the mask as figure 2. The agreement between theory and experiment is excellent, with a few exceptions. As mentions before the left edge of the experimental data is moved inwards slightly. At 2080 nm the central 7 orders are almost fully visible in the simulation as compared to the experiment data showing only the left side. This is probably due to an inaccuracy in the mask position. Inaccuracies can be caused by noise in the relation between the piezoelectric transducer voltage and the mask position

Overall the path integral simulation represents the experimental data, in agreement with quantum mechanics. Moving the mask to block one of the slits does not give anything unexpected and we see exactly what quantum mechanics predicts.

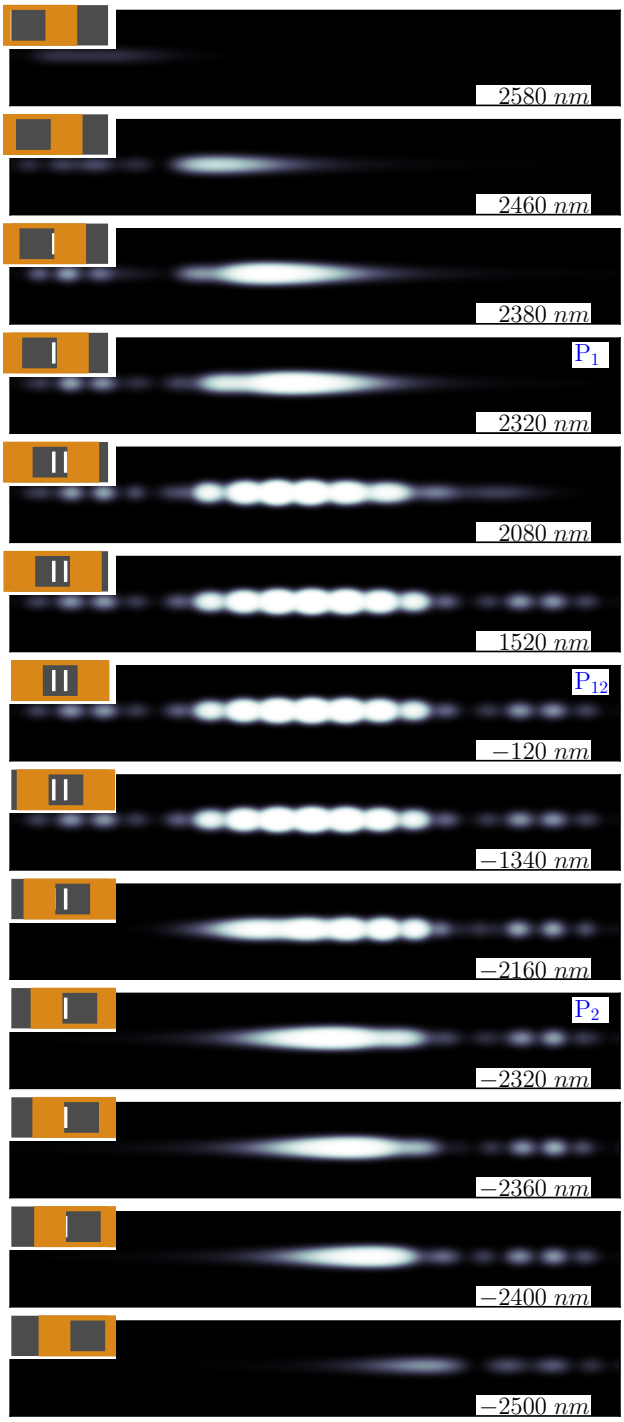

Figure S3. Mask movement simulation. A mask is moved over a double-slit (inset) and the resulting probability distributions are shown. The mask allows the blocking of one slit, both slits, or neither slit in a non destructive way. The individual slits are 62 nm wide and separated by 272 nm. The mask has a 4.5 μm wide opening. The labeled dimensions are the positions of the center of the mask.

References

[S1] Barwick B, Gronniger G, Lu Y, Liou S Y and Batelaan H 2006 A measurement of electron-wall interaction using transmission diffraction from nanofabricated gratings *J. Appl. Phys.* **100** 074322

[S2] Born M and Wolf E 1980 *Principles of Optics* (Pergamon, Oxford) 6th ed Chap X

[S3] Feynman R P 1948 Space-Time approach to non-relativistic quantum mechanics *Rev. Mod. Phys* **20** 367

[S4] Caprez A, Bach R, McGregor S and Batelaan H 2009 A wide-angle electron grating bi-prism beam splitter *J. Phys. B* **42** 165503